A Model for the Peak-Interval Task Based on Neural Oscillation Delimited States

Thiago T. Varella[1,2], Marcelo Bussotti Reyes[3], Marcelo S. Caetano[3,4], Raphael Y. de Camargo[3*]

[1]Princeton Neuroscience Institute, Princeton University, Princeton, NJ, USA
[2]Universidade de São Paulo, São Paulo, SP, Brazil
[3]Center for Mathematics, Computing and Cognition, Universidade Federal do ABC, São Bernardo do Campo, SP, Brazil
[4]Instituto Nacional de Ciência e Tecnologia sobre Comportamento, Cognição e Ensino, Brazil.

[*]To whom correspondence should be addressed; e-mail: raphael.camargo@ufabc.edu.br

Timing mechanisms in the brain are still an open issue. Several existing computational models for timing can reproduce properties of experimental psychophysical responses. Still, only a few consider the underlying biological mechanisms, such as the synchronized neural activity that occurs in several brain areas. In this paper, we introduce a model for the peak-interval task based on neuronal network properties. We consider that Local Field Potential (LFP) oscillation cycles specify a sequence of states, represented as neuronal ensembles. Repeated presentation of time intervals during training reinforces the connections of specific ensembles to downstream networks. Later, during the peak-interval procedure, these downstream networks are reactivated by previously experienced neuronal ensembles, triggering actions at the learned time intervals. The model reproduces experimental response patterns from individual rats in the peak-interval procedure, satisfying relevant properties such as the Weber law. Finally, the model provides a biological interpretation of its parameters.

Introduction

How does the brain process time-related tasks? There seem to be different mechanisms for different time scales (*Buhusi and Meck, 2005, Paton and Buonomano, 2018*). The microsecond range relates to behaviors such as interaural delay (*Shaffer, 1984*). Circadian rhythms (*Czeisler, 1999*) are essential

to biological processes found in nature such as human body temperature (*Benloucif et al., 2005*). The interval timing includes from tens of milliseconds to tens of minutes. This interval stands out in many aspects of animal behavior and physiology. Examples include foraging, decision making, sequential motor performance, and associative conditioning (*Merchant and Lafuente, 2014*).

There exists several models for interval timing that reproduce behavioral results, but few of them could describe simultaneously the critical properties of timing observed in experimental data (*Maniadakis and Trahanis, 2014*). The most influential model was the SET model (*Gibbon, 1977*) given its success with the scalar property (*Grondin, 2014*). One possible mechanism for the SET model is the Pacemaker and Accumulator, in which a clock emits pulses stored by an accumulator. Another example is the striatal beat frequency (SBF) model (*Matell and Meck, 2004, Oprisan and Buhusi, 2011*), where the coincidental activation of neurons is used to perceive time using specific oscillations.

Despite the effort over the years to find a central abstract mechanism that integrates many different tasks related to timing, most of the evidence today points to mechanisms related to the dynamics of neural populations (*Paton and Buonomano, 2018, Balci and Simen, 2016, Eichenbaum, 2014*). We can define the state of a network as the set of active neurons at a given moment. With state-dependent networks (*Karmarkar and Buonomano, 2007*), a downstream network can use the state trajectory evolution of a given network to measure time intervals. Despite several successful predictions, such as the reproduction of ramping activity (*Durstewitz and Deco, 2008, Machens et al., 2005*), only recently it was found a recurrent neural network on the model that could satisfy the Weber Law (*Hardy and Buonomano, 2018*).

The LeT model (*Machado, 1997, Machado et al., 2016*) consists of a vector of associative links for different states that activates serially when trying to estimate a certain time. Each state has an output weight that is adjusted by reinforcements during the learning of the time interval. The model can reproduce many essential features of the timing literature, such as the scalar property. But there are no direct biological correlates for this model.

Recent results suggest that natural brain oscillations have a crucial role in the hippocampus (*Klimesch, 1999, Belluscio et al., 2012*), the thalamus (*Steriade et al., 1993*), striatum (*Berke et al., 2004*), amygdala (*Halgren et al., 1977*), and other areas. Areas such as the hippocampus appear to operate on sequences of states (*Lisman et al., 2005, Buzsáki and Tingley, 2018*), which could be chained using heteroassociative rules (*Sompolinsky and Kanter, 1986, de Camargo et al., 2018*). This brain area is also important to time-related tasks (*Meck et al., 1984*), and have neurons, called time cells (*Eichenbaum, 2014*), that fire in specific moments in a time estimation task. This kind of cell was also found in the medial entorhinal cortex (MEC) (*Tsao et al., 2018*) and medial prefrontal cortex (mPFC) (*Tiganj et al., 2017*). A recent proposal is that time is not explicitly represented in the brain and are just a byproduct of ongoing tasks, composed as a succession of events (*Buzsáki and Llinas, 2017*). This proposal is compatible with the idea of using chain of events to perform time-related tasks.

In this article, we present a timing model inspired on brain networks with oscillatory activity and sequential state activation, with states represented as neuronal ensembles delimited by oscillatory cy-

cles. We model a peak-interval procedure, where repeated presentation of time intervals during training reinforces the connections of specific ensembles to a downstream network. Later, during the reproduction phase, these downstream networks are reactivated by previously experienced neuronal ensembles, triggering actions at the learned time intervals. The implementation of this model is similar to the Learning-to-time model, providing a biological interpretation of this model.

Methods

We first describe the Peak-Interval Procedure in rats. Then, we explain how we model the behavior of rats in this task.

Peak-Interval Procedure We collected the data using the Peak-Interval Procedure, as shown in Figure 1. We trained six Sprague Dawley rats initially to press a lever in a standard operant chamber to receive a food pellet (fixed-ratio 1 schedule of reinforcement for one experimental session). Next, we trained the rats to make a nose-poke response 20 seconds after the lever press in order to receive the food pellet (*tandem* fixed ratio 1/fixed interval 20 s schedule of reinforcement). During this phase, each trial initiated by the onset of a houselight. The first lever press after light onset initiated a 20-s fixed interval. Food was primed 20 s after the first lever press. The first head entry into the food cup (detected by the breaking of a photobeam) after food prime delivered the food pellet, terminated the houselight, and introduced a variable inter-trial interval (ITI = 40 s). If no head entries were made within 20 s from food prime, the houselight turned off, we initiated the ITI, but there was no food delivered. We trained the rats for 98 experimental sessions in this phase to ensure behavior stability. Finally, in the last training phase, we introduced peak trials with a probability of .5. During peak trials, the houselight remained on for another 60 s after food prime, during which we recorded the responses (lever presses and head entries), but there was no food pellets. After 60 s from food prime, we terminated the houselight, introduced the ITI, and started the next trial.

Learning Mechanism Model The model consists of a heteroassociative network represented by a series of successive states (*Sompolinsky and Kanter, 1986, de Camargo et al., 2018*). Each state corresponds to a subset of active neural units within a Local Field Potential (LFP) oscillation. Each state i has a synaptic weight w_i connecting it to a downstream network. The weights store information about the specific time being learned, causing the downstream network to fire at that specific time. The model has two phases to account for the resetting of the downstream network for different time tasks: the learning phase and the reproduction phase.

During the learning phase, states are consecutively activated until a specific target time T has elapsed (Figure 2a). At that moment, the synaptic weight w_i between the current active state i and the downstream network increases one unit. This state activation sequence happens multiple times, one for each learning trial. For each trial, there is a transition time step t_s between states drew from a Gaussian distri-

bution with mean μ and standard deviation σ. At the end of the simulation, we normalized the w_i values so that the maximum weight is 1.

Algorithm 1 Learning phase

- Parameters: μ, σ and T.
- Initialize vector w, with $w_i = 0, \forall i$.
- For each trial:
  1. Initialize the elapsed time $t = 0$ and active state $i = 0$.
  2. Draw a time step t_s from the normal distribution $N(\mu, \sigma)$
  3. While $t < T$, update $t = t + t_s$ and $i = i + 1$.
  4. Add 1 to w_i.
- Divide vector w by $maximum(w_i), \forall i$.

Note that the last activated state i after the elapsed time T is $\frac{T}{t_s}$. Thus, the function that describes the weight w_i converges to a distribution obtained by a change of variables. The change is from the Gaussian distribution of t_s to $i = \frac{T}{t_s}$. Prior to normalization, we can describe the distribution as:

$$f(i, \mu, \sigma) = \frac{T}{i^2\sqrt{2\pi\sigma^2}} \exp\left[\frac{-\left(\frac{T}{i} - \mu\right)^2}{2\sigma^2}\right] \tag{1}$$

We then reduce the parameters μ and σ to the coefficient $\rho = \sigma/\mu$. When we change the parameters of the states i to the pressing time using the transformation $t = \mu \cdot i$, and make $\sigma = \mu\rho$, Equation 1 becomes:

$$f(i, \mu, \sigma) = f\left(\frac{t}{\mu}, \mu, \mu\rho\right) = \frac{1}{\mu^2}\frac{T}{t^2\sqrt{2\pi\rho^2}} \exp\left[-\frac{(\frac{T}{t} - 1)^2}{2\rho^2}\right] = \frac{1}{\mu^2} f\left(t, 1, \rho\right)$$

The threshold ℓ is the lower degree of activation that generates the behavioral response, and it ranges from 0 to 1. Thus, we have to normalize the maximum weight to 1 (last step in Algorithm) to establish a comparison of w_i and ℓ. Given the maximum $M(\rho)$ of the function $f(t, 1, \rho)$, we have that $\frac{M(\rho)}{\mu^2}$ must be the maximum of the function $f(i, \mu, \sigma)$. The final function describing the neural activity at the network in terms of the time elapsed is

$$(f(t, \mu, \sigma))_{\ell\in[0,1]} = \frac{\mu^2}{M(\rho)}\frac{1}{\mu^2} f\left(t, 1, \rho\right) = \frac{T}{M(\rho)t^2\sqrt{2\pi\rho^2}} \exp\left[-\frac{(\frac{T}{t} - 1)^2}{2\rho^2}\right] \tag{2}$$

so we can conclude that the only relevant parameters of the model are ρ and ℓ.

Behavioral Reproduction In the reproduction phase, the model uses the same series of states (Figure 2b). When the network activates states with output weights lower than a threshold $0 \leq \ell \leq 1$, the behavioral response for the Peak-Interval (PI) Procedure is to induce pressing in a basal rate r_b. When

it reaches states with weights larger than the threshold, the response is in a higher rate r_a. Algorithm 2 shows the simulation steps.

We used the reproduction phase algorithm to generated single trials responses. We sampled the hypothetical presses using a Poisson distribution with average rate $\lambda = r_a$ between time to start burst t_1 and time to stop burst t_2, and $\lambda = r_b$ for the remaining period.

Algorithm 2 Reproduction phase

- Parameters μ, σ, w, ℓ, r_b and r_a.
- For each trial:
  1. Initialize the elapsed time $t = 0$ and active state $i = 0$.
  2. Draw a time step t_s from the normal distribution $N(\mu, \sigma)$
  3. While $w_i \leq \ell$
     Update $t = t + t_s$ and $i = i + 1$.
  4. $t_1 = t$.
  5. While $w_i \geq \ell$
     Update $t = t + t_s$ and $i = i + 1$.
  6. $t_2 = t$.
  7. Generate pressing times from 0 to t_1 from Poisson process with a rate r_b
  8. Generate pressing times from t_1 to t_2 from a Poisson process with a rate r_a
  9. Generate pressing times from t_2 till end from a Poisson process with a rate r_b

Parameters to Fit We performed a parameter search for each rat separately. Parameters $\rho = \sigma/\mu$ and ℓ are important to the neural mechanism, while r_a and r_b are important to the behavioral response of rats.

Given each of these 4 parameters, we repeated some trials of the reproduction phase. For each trial, we found a set of lever-pressing times and calculated a time histogram similar to Figure 1(b) using 80 bins (1 bin per second).

We found the best fit by calculating the Euclidian distance between the model and one specific rat. The difference was between the experimental and the model vector. The experimental vector contained each 1-second bin of the experimental lever press distribution of a rat. The model vector contained each 1-second bin of the distribution generated by the model. After calculating the difference for many possible parameters for the model, we stored the parameters that gave the lower distance.

The basal rate and the burst rate were found by analyzing each distribution for each rat. That way, we made sure that the model parameters would be compatible with the model behavior. For example, we ensured that the basal rate would be similar to the limiting pressing rate given by the tail of the experimental distributions. We searched the other two parameters (ρ and ℓ) in a grid where both parameters ranged from 0 to 1 in intervals of 0.05.

Weber Law With the best parameters it is possible to check the validity of the scalar property. To assess the scalar property, we need to change the target time. For each target time, we simulated the model 10 times and averaged the standard deviation of the resulting pressing distributions given by the model. Only 10 times was enough because the distributions had little variation in each simulation.

Lever presses associated during the basal response influence the response distributions to be above the zero line, i.e., the responses distribution do not converge to zero at their tails. Hence, we are not able to normalize these curves and neither calculate their associated statistics. For that reason, we considered only the responses during the bursts to calculate the standard deviations.

Individual trials Once you found a burst rate (r_a), a basal rate (r_b), a time to start (t_1) and a time to stop (t_2) the burst, it is possible to generate a single trial using the Algorithm 2. The parameters we used to generate a set of single trials for each rat were the same parameters obtained from the best fit.

To compare the onset (t_1) and offset (t_2) of the burst of the model with the equivalent from the experimental distributions (bin size = 1 second) we fitted each experimental trial using the methodology proposed by (*Church et al., 1994*). In that method, we made a search within t_1 and t_2 and stored the values that gave the maximum value of

$$t_1(r - r_1) - (t_2 - t_1)(r - r_2) + (80 - t_2)(r - r_3) \tag{3}$$

where r is the pressing rate for the whole trial, r_1 is the pressing rate for the first interval (from 0 to t_1), r_2 is the pressing rate for the second interval (that is equivalent to the burst rate, from t_1 to t_2) and r_3 is the pressing rate in the last interval (from t_2 to 80).

Results

Reproduction of behavioral responses The model reproduced the experimental pressing rate response of 6 individual rats (Figure 3a). We characterized the pressing rate by tuning 4 parameters: the $\rho = \sigma/\mu$ ratio, the threshold ℓ of the neural network, the burst rate r_a, and the basal rate r_b. We selected the parameters by minimizing the Euclidean distance (Table 1) between the simulated and experimental responses. Except for rat 3, all simulations could reproduce the target time and the standard deviation of the curve.

Each rat had a different pressing rate. We considered in the model that the rat would press at the burst rate r_a when the downstream neural network is active. Otherwise, it would press at the basal rate r_b. The target time T is the most important factor to determinate the activation of the downstream network. The threshold ℓ and the coefficient $\rho = \sigma/\mu$ of the time step sizes dictated the deviation of the final distribution. They are responsible for a fine-tuning of the response curve.

Notice that the rat 3 had the highest Euclidean distance. That difference happens because the peak of the response distribution is delayed in relation to the peak predicted by the model.

Table 1: Euclidean distance between the experimental data and the best fitted model for each rat

Rat	1	2	3	4	5	6
Distance	0.86	1.06	1.14	0.58	0.91	0.64

Parameters similarities The parameters σ/μ ratio and ℓ obtained for each of the rats were similar. Within the space of parameters, we plotted the regions where the Euclidean distance of the model and the experimental data were less than a certain value (Figure 3b). The smallest Euclidean distance that gave us an intersecting region is approximately 1.2. The parameters correspondent to that distance are $(\ell, \rho) = (0.125, 0.35)$

The basal rate found for each rat was, respectively, 0.3, 0.15, 0.02, 0.2, 0.1 and 0.19. The burst rate used for each rat was, respectively, 1.7, 2.1, 1.3, 1.8, 2.2, 1.3. Notice that basal rates were similar between rats, as were burst rates. The basal rates correspond to the height of the pressing rate curves at the immediate beginning and during the end of the sessions.

Weber Law There was a linear relationship between the target time and the standard deviation of the responses given by the model (Figure 3c). The error within the standard deviations (y-axis) was small and thus not visible in the graph. The Weber fraction WF calculated using the parameters given by the intersecting region of the six rats was $WF = 0.5$. The value is consistent with values found in the literature, such as the range of 0.35 to 0.5 in (*Gibbon, 1977*).

Start and stop time distributions The distributions of start and stop times that the model generated were similar to the experimental distributions (Figures 4a,b). We simulated single trials using Algorithm 2 for each rat. The parameters used were those from the best fit. The number of trials simulated was proportional to the experimental number of trials for each rat. The model reproduced the peak positions. It could not reproduce well the right tail of the start bursts and left tail of stop bursts. Figures 4c and 4d compare model-generated and experimental data, respectively, from one rat.

Discussion

The proposed model works with neural networks that generate reproducible sequences of states at steady rates. Heteroassociative networks (*Sompolinsky and Kanter, 1986, de Camargo et al., 2018*) can be used to implement our model as a biological neural network, as well as Synfire chains (*Abeles, 1991, Miyata et al., 2013*). The later introduced the idea of a rapid sequential activation of groups of neurons, representing the states in our model. Accordingly, heteroassociative networks are promising as a biological implementation of the model, since they can produce long sequences of state activation within a single network while performing pattern completion (*de Camargo et al., 2018*). This kind of networks are present in both the CA3 (*Lisman et al., 2005*) and CA1 (*Miyata et al., 2013*) subregions of the hippocampus, which is involved in some time-related tasks (*Meck et al., 1984*). Accumulated evidence

suggests that timing mechanisms are decentralized () and the hippocampus is one from brain areas where sequences of states could be evoked.

Neural activity oscillations are the main candidate for providing the steady state transition rates. Subsequent states could be represented on consecutive oscillatory cycles. The parameter μ in our model would be the oscillation period and σ its variability. Interestingly, the coefficient $\rho = \sigma/\mu$ of the oscillation - not the Weber fraction - could be important to characterize brain oscillations, for instance, indicating its adaptability in certain contexts (*Schlee et al., 2014, Calomeni et al., 2017*). The parameters obtained from the intersection of the 6 rats (Figure 3b) predicted a coefficient ρ at approximately 0.35. This could correspond, for instance, to $\mu = 25ms$ and $\sigma = 8.75ms$, resulting in a frequency range of 30-60Hz, in the range of experimentally observed slow gamma waves (*Belluscio et al., 2012*). Gamma frequency waves are present in several brain areas and could be a candidate for providing the state transition rates.

The reproducible sequences of states at steady rates would also give rise to cells that respond at specific times of the task, similarly to time cells, discovered in the Hippocampus (*Einchenbaum, 2013*), medial entorhinal cortex (MEC) (*Tsao et al., 2018*) and medial prefrontal cortex (mPFC) (*Tiganj et al., 2017*). Neurons with behavior similar to time cells could appear both as part of the states in the sequence and as part of the downstream network. These time cells would also "retime" when an important temporal parameter changes. (*MacDonald et al., 2011*). The existence of neurons with time cells is an important link of the proposed model with existing biological evidence.

The proposed model uses a bottom-up approach, from properties of brain neural networks to behavioral responses from rats. Interestingly, it has a similar a similar computational implementation with the Learning-to-Time (LeT) behavioral model. In both models, serially activated states have different link strengths to an outside unit, and a threshold leading to behavioral responses. There are differences, such as the LeT use of extinguishing of non-active link strengths. The LeT model was motivated by the proposal of behavioral internal states, without reference to the underlying biological mechanisms. Our proposed model can provide a link from the behavioral model to a possible biological substrate.

The model has some limitations. The model could not reproduce perfectly the start and the stop distributions of burst press activities (Figure 4). That could be happening because of the way we are reproducing single trials. With Figure 4c and d, we concluded that the experimental data is more sparsely distributed than the way we model it in the simulation. That difference comes from the fact that the neural network we are proposing deals with the task-related interval representation in the brain. The way the behavior appears will have more intricate mechanisms. For example, the constraint of one burst per trial is not true in all experimental responses.

Another limitation is that there is not a source of bias in our model. Bias could arise from impulsive responding (*Matell and Portugal, 2007, Renda et al., 2014*), for example. The model does not capture correctly the pressing rate distribution of rat 3, whose peak response lies 5 to 10 seconds delayed from the target time. The peak of the distribution of simulated responses depends on the target time learned by the rat. One way to account for a variation in the distribution peak would be the addition of a bias.

That bias would change the encoding of the neural network to the response rate, and thus change the time between two neural states in the behavioral reproduction phase. Even so, since the bias is more related to the decision-making process than the timing mechanism itself, we decided to not include this parameter and thus reduce the complexity of the model.

Acknowledgements

During the project, TTV was supported by the Fundação de Amparo à Pesquisa do Estado de São Paulo (FAPESP, grant #2016/19691-1) and by the Universidade de São Paulo International Cooperation Office Scholarship. MSC is a member of the Instituto Nacional de Ciência e Tecnologia sobre Comportamento, Cognição e Ensino, with support from the Brazilian National Research Council (CNPq, Grant #465686/2014-1), the Coordination of Superior Level Staff Improvement (CAPES, Grant #88887.136407/2017-00), and FAPESP (Grant #2014/50909-8). The authors would like to thank the members of the Timing and Cognition Lab (http://neuro.ufabc.edu.br/timing/), at Universidade Federal do ABC, for their suggestions during project development.

References

Abeles, 1991. Abeles, M. (1991). *Corticonics: neuronal circuits of the cerebral cortex*. Cambridge: Cambridge University Press.

Balci and Simen, 2016. Balci, F. and Simen, P. (2016). A decision model of timing. *Current Opinion in Behavioral Sciences*, 8:94–101.

Belluscio et al., 2012. Belluscio, M. A., Mizuseki, K., Schimdt, R., Kempter, R., and Buzsáki, G. (2012). Cross-frequency phase–phase coupling between theta and gamma oscillations in the hippocampus. *The Journal of Neuroscience*, 32(2):423–435.

Benloucif et al., 2005. Benloucif, S., Guico, M. J., Reid, K. J., Wolfe, L. F., L'Hermite-Balériaux, M., and Zee, P. C. (2005). Stability of melatonin and temperature as circadian phase markers and their relation to sleep times in humans. *Journal of Biological Rhythms*, 2:178–188.

Berke et al., 2004. Berke, J. D., Okatan, M., Skurski, J., and Eichenbaum, H. (2004). Oscillatory entrainment of striatal neurons in freely moving rats. *Neuron*, 43:883–896.

Buhusi and Meck, 2005. Buhusi, C. V. and Meck, W. H. (2005). What makes us tick? functional and neural mechanisms of interval timing. *Nature Reviews Neuroscience*, 6:755–765.

Buzsáki and Llinas, 2017. Buzsáki, G. and Llinas, R. (2017). Space and time in the brain. *Science (New York, N.Y.)*, 358(6362):482–485.

Buzsáki and Tingley, 2018. Buzsáki, G. and Tingley, D. (2018). Space and Time: The Hippocampus as a Sequence Generator. *Trends in Cognitive Sciences*, 22(10):853–869.

Calomeni et al., 2017. Calomeni, M. R., da Silva, V. F., Velasques, B. B., Feijó, O. G., Bittencourt, J., and de Souza e Silva, A. P. R. (2017). Modulatory effect of association of brain stimulation by light and binaural beats in specific brain waves. *Clin Pract Epidemiol Ment Health*, 13:134–144.

Church et al., 1994. Church, R., Meck, W., and Gibbon, J. (1994). Application of scalar timing theory to individual trials. *Journal of Experimental Psychology Animal Behavior Processes*, 20(2):135–155.

Czeisler, 1999. Czeisler, C. A. e. a. (1999). Stability, precision, and near-24-hour period of the human circadian pacemaker. *Science*, 284:2177–2181.

de Camargo et al., 2018. de Camargo, R., Recio, R. S., and Reyes, M. B. (2018). Heteroassociative storage of hippocampal pattern sequences in the ca3 subregion. *PeerJ*, 6:e4204.

Durstewitz and Deco, 2008. Durstewitz, D. and Deco, G. (2008). Computational significance of transient dynamics in cortical networks. *The European journal of neuroscience*, 27 1:217–27.

Eichenbaum, 2014. Eichenbaum, H. (2014). Time cells in the hippocampus: a new dimension for mapping memories. *Nature Reviews Neuroscience*, 15(11):732–744.

Einchenbaum, 2013. Einchenbaum, H. (2013). Memory on time. *Trends in Cognitive Sciences*, 17(2):255.

Gibbon, 1977. Gibbon, J. (1977). Scalar expectancy theory and weber's law in animal timing. *Psychological Review*, 84(3):279–325.

Grondin, 2014. Grondin, S. (2014). About the (non)scalar property for time perception. *Advances in Experimental Medicine and Biology*, 829.

Halgren et al., 1977. Halgren, E., Babb, T., and Crandall, P. (1977). Responses of human limbic neurons to induced changes in blood gases. *Brain Res.*, 132:43–63.

Hardy and Buonomano, 2018. Hardy, N. F. and Buonomano, D. V. (2018). Encoding time in feedforward trajectories of a recurrent neural network model. *Neural Computation*, 30:378–396.

Karmarkar and Buonomano, 2007. Karmarkar, U. and Buonomano, D. (2007). Telling time in the absence of clocks. *Neuron*, 53(3):427–438.

Klimesch, 1999. Klimesch, W. (1999). Eeg alpha and theta oscillations reflect cognitive and memory performance: a review and analysis. *Brain Research Reviews*, 29:169–195.

Lisman et al., 2005. Lisman, J. E., Talamini, L., and Raffone, A. (2005). Recall of memory sequences by interaction of the dentate and ca3: a revised model of the phase precession. *Neural Networks*, 18(9):1191–1201.

MacDonald et al., 2011. MacDonald, C. J., Lepage, K. Q., and Eden, U.W., E. H. (2011). Hippocampal "time cells" bridge the gap in memory for discontiguous events. *Neuron*, 71(4):737–749.

Machado, 1997. Machado, A. (1997). Learning the temporal dynamics of behavior. *Psychological Review*, 104(2):241–265.

Machado et al., 2016. Machado, A., Carvalho, M. P., and Tonneau, F. (2016). Learning in the temporal bisection task: Relative or absolute? *Journal of Experimental Psychology: Animal Learning and Cognition*, 42(1):67–81.

Machens et al., 2005. Machens, C. K., Romo, R., and Brody, C. D. (2005). Flexible control of mutual inhibition: a neural model of two-interval discrimination. *Science*, 307 5712:1121–4.

Maniadakis and Trahanis, 2014. Maniadakis, M. and Trahanis, P. (2014). Time models and cognitive processes: a review. *Frontiers in neurorobotics*, 8.

Matell and Meck, 2004. Matell, M. S. and Meck, W. H. (2004). Cortico-striatal circuits and interval timing: coincidence detection of oscillatory processes. *Cognitive Brain Research*, 21:139–170.

Matell and Portugal, 2007. Matell, M. S. and Portugal, G. S. (2007). Impulsive responding on the peak-interval procedure. *Behavioral Processes*, 74(2):198–208.

Meck et al., 1984. Meck, W. H., Church, R., and D.S., O. (1984). Hippocampus, time, and memory. *Behavioral Neurosciencel*, 98(1):3–22.

Merchant and Lafuente, 2014. Merchant, H. and Lafuente, V. (2014). Introduction to the neurobiology of interval timing. *Advances in Experimental Medicine and Biology*, 829.

Miyata et al., 2013. Miyata, R., Ota, K., and Aonishi, T. (2013). Optimal design for hetero-associative memory: Hippocampal ca1 phase response curve and spike-timing-dependent plasticity. *PLoS One*, 8(10).

Oprisan and Buhusi, 2011. Oprisan, S. A. and Buhusi, C. V. (2011). Modeling pharmacological clock and memory patterns of interval timing in a striatal beat-frequency model with realistic, noisy neurons. *Frontiers in Integrative Neuroscience*, 5.

Paton and Buonomano, 2018. Paton, J. J. and Buonomano, D. V. (2018). The neural basis of timing: Distributed mechanisms for diverse functions. *Neuron*, 98:687–706.

Renda et al., 2014. Renda, C. R., Stein, J. S., and Madden, G. J. (2014). Impulsive choice predicts poor working memory in male rats. *PLOS One*, 9(4).

Schlee et al., 2014. Schlee, W., Schecklmann, M., Lehner, A., Kreuzer, P. M., Vielsmeier, V., Poeppl, T. B., and Langguth, B. (2014). Reduced variability of auditory alpha activity in chronic tinnitus. *Neural Plasticity*, 436146.

Shaffer, 1984. Shaffer, H. (1984). Timing and time perception. *The New York Academy of Sciences*, 423:420–428.

Sompolinsky and Kanter, 1986. Sompolinsky, H. and Kanter, I. (1986). Temporal association in asymmetric neural networks. *Phys Rev Letters*, 57(22).

Steriade et al., 1993. Steriade, M., McCormick, D. A., and Sejnowski, T. J. (1993). Thalamocortical oscillations in the sleeping and aroused brain. *Science*, 262 5134:679–85.

Tiganj et al., 2017. Tiganj, Z., Jung, M. W., Kim, J., and Howard, M. W. (2017). Sequential firing codes for time in rodent medial prefrontal cortex. *Cerebral Cortex*, 27(12):5663–5671.

Tsao et al., 2018. Tsao, A., Sugar, J., Lu, L., Wang, C., Knierim, J. J., Moser, M.-B., and Moser, E. I. (2018). Integrating time from experience in the lateral entorhinal cortex. *Nature*, 561:57–62.

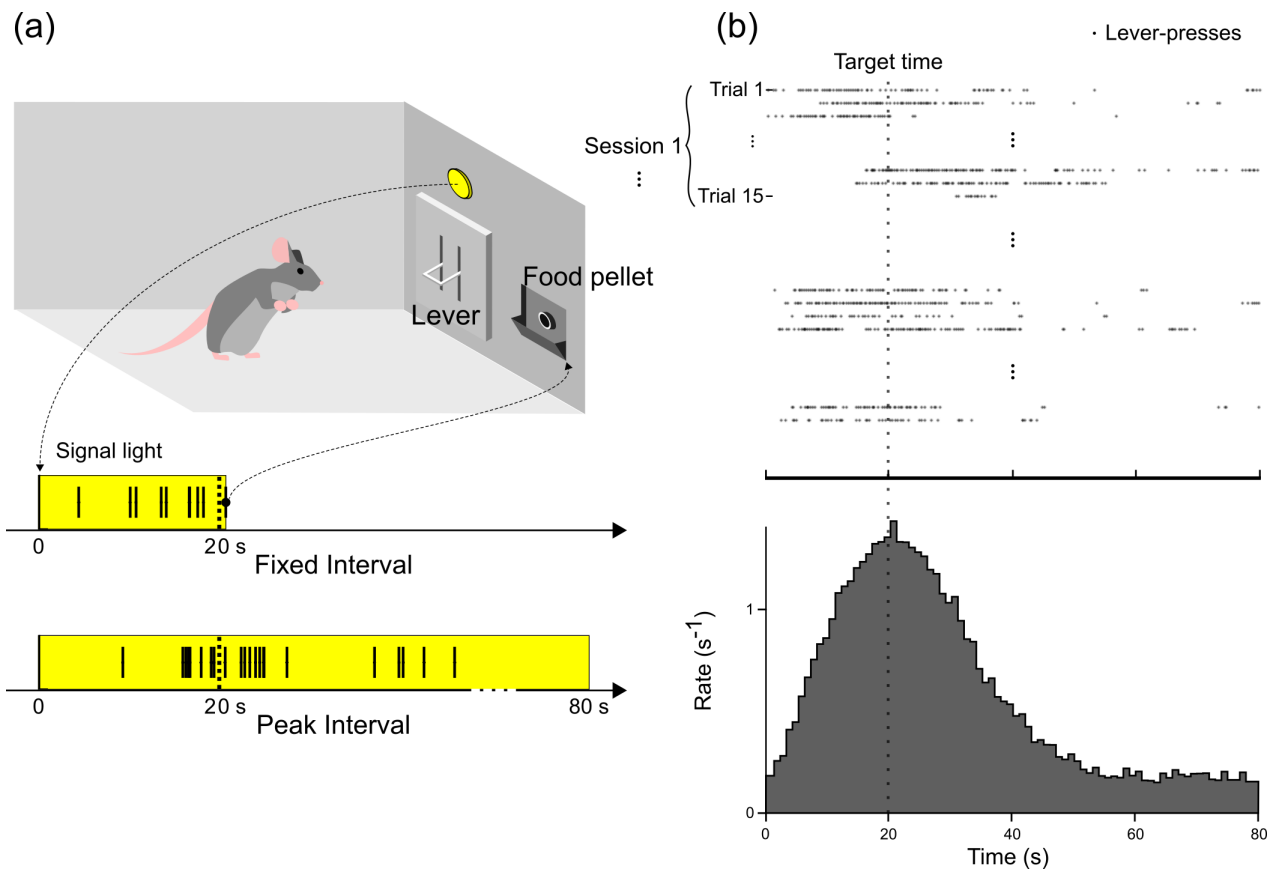

Figure 1: (a) Experimental setup of a typical Peak-Interval Procedure during a Fixed-Interval trial. A time-dependent light will be used as a stimulus and at the first lever press after 20 seconds the light will turn off and the food will drop at the food pellet. During a peak-interval, the light will keep turned on and the food will not drop. (b) Summary of the presses registered during each peak-interval trial with a target time of 20 s and the distribution containing the mean number of presses during each second of a trial.

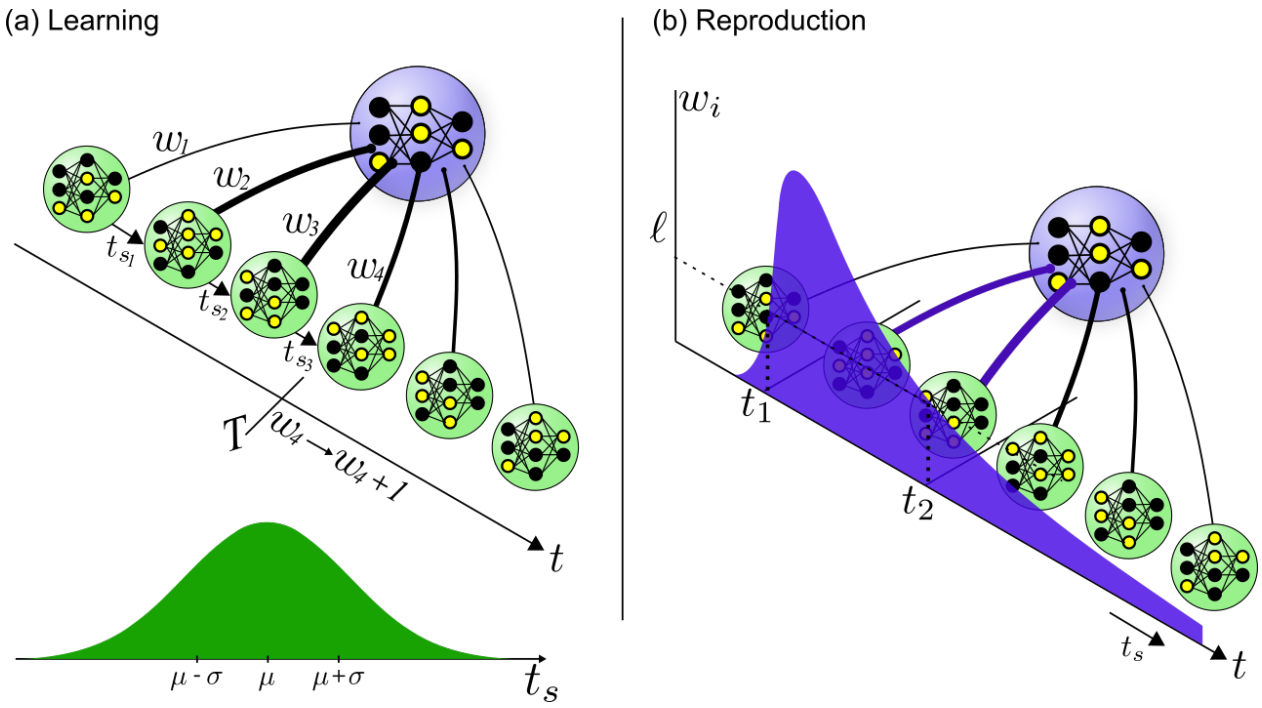

Figure 2: (a) Visual representation of the Learning Phase of the model. Each green sphere represents a state and the lines between the green and the blue spheres represent the weight w_i of the link between the state itself and a specific other neural unit represented by the blue sphere. The time steps t_s compose a Gaussian distribution and the time t increases according to these steps. When the time t reaches the target time T, the weight of current state will raise. (b) Visual representation of the Reproduction Phase of the model. The same states will be activated successively just like the learning phase but linked with a basal response. While the process reaches states with weights above a threshold ℓ, it will activate a neural unit responsible to identify the target time.

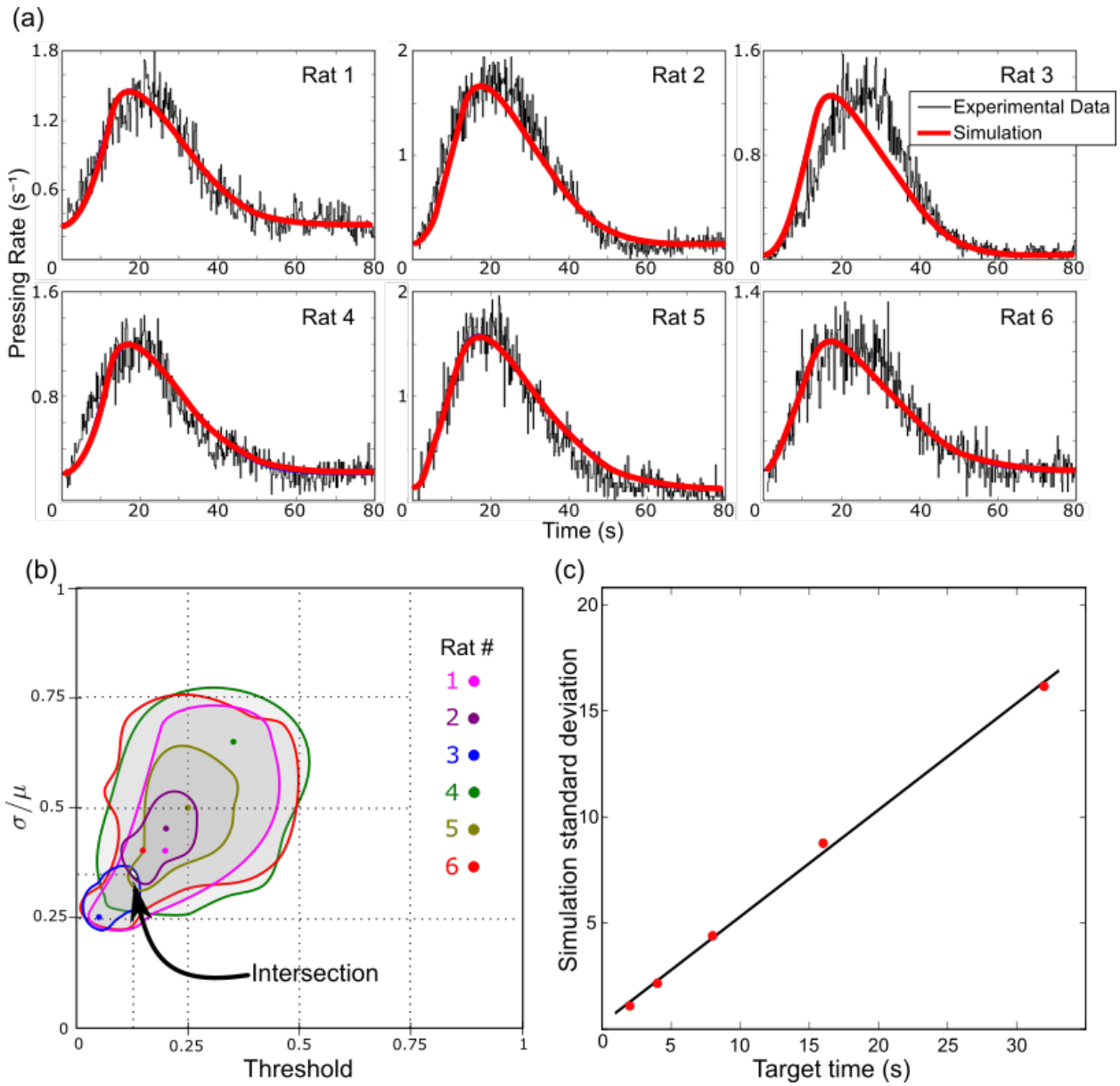

Figure 3: (a) Fitting of the model with the experimental data for each of the 6 rats. The red line represents the simulation fitted with the best parameters and the black line represents the experimental data. (b) Region in the space of parameters in which the goodness of fit measured by the Euclidean Distance between the simulation and the actual data was smaller than 1.2. Each color represents a different rat. The solid dots represent the minimum distance (best goodness of fit). (c) Reproduction of the scalar property by calculating the standard deviation for different target times and then plotting a linear regression.

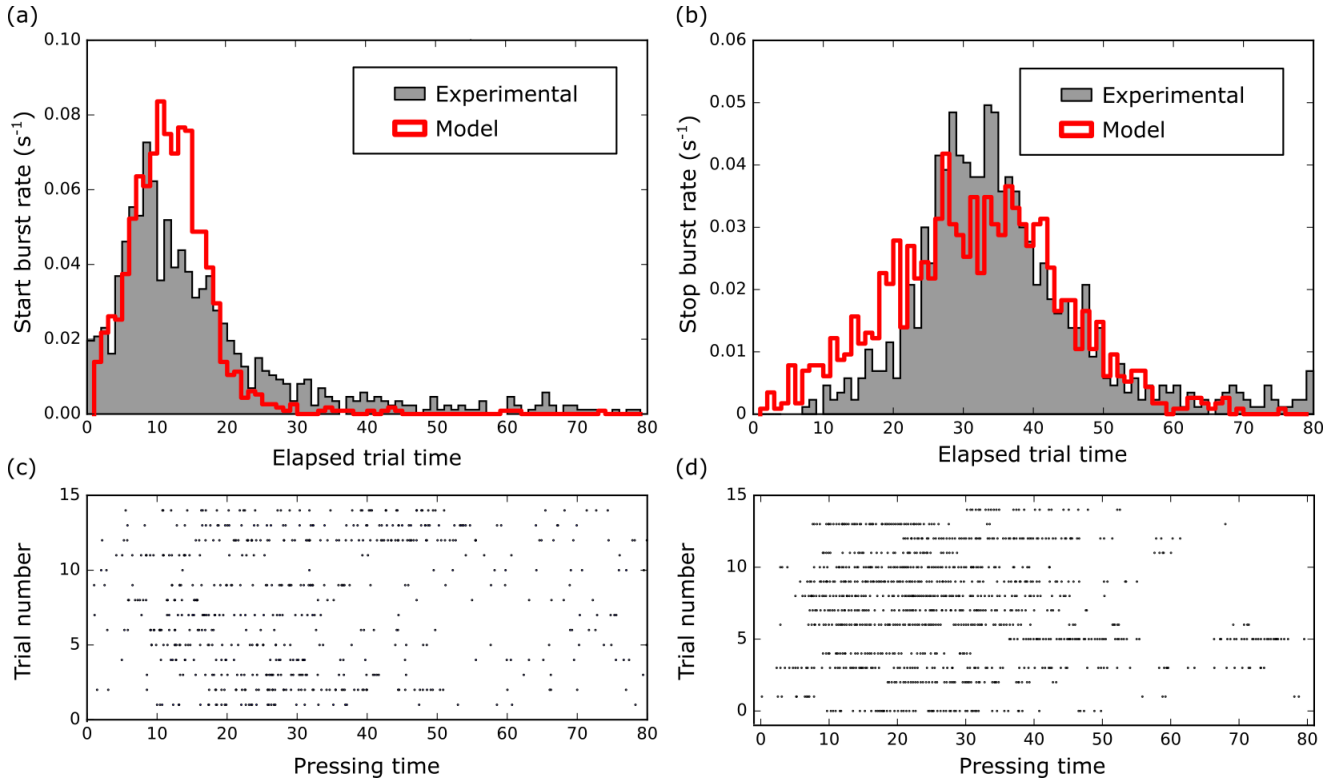

Figure 4: (a) Comparison between start-times distribution in individual trials, both from experimental data (gray) and generated by the model (red). (b) Same as (a) for stop-times. (c) Individual trials generated by the model using the parameters optimized from rat 2. (d) Individual trials for rat 2, session 11.